Nonadditive Compositional Curvature Energetics of Lipid Bilayers

A. J. Sodt,[1,*] R. M. Venable,[1] E. Lyman,[2] and R. W. Pastor[1]
[1]National Heart, Lung, and Blood Institute, National Institutes of Health, Bethesda, 20892 Maryland, USA
[2]Department of Physics and Astronomy and Department of Chemistry and Biochemistry, University of Delaware, Newark, 19716 Delaware, USA

(Received 29 April 2016; revised manuscript received 26 July 2016; published 23 September 2016)

The unique properties of the individual lipids that compose biological membranes together determine the energetics of the surface. The energetics of the surface, in turn, govern the formation of membrane structures and membrane reshaping processes, and thus they will underlie cellular-scale models of viral fusion, vesicle-dependent transport, and lateral organization relevant to signaling. The spontaneous curvature, to the best of our knowledge, is always assumed to be additive. We describe observations from simulations of unexpected nonadditive compositional curvature energetics of two lipids essential to the plasma membrane: sphingomyelin and cholesterol. A model is developed that connects molecular interactions to curvature stress, and which explains the role of local composition. Cholesterol is shown to lower the number of effective Kuhn segments of saturated acyl chains, reducing lateral pressure below the neutral surface of bending and favoring positive curvature. The effect is not observed for unsaturated (flexible) acyl chains. Likewise, hydrogen bonding between sphingomyelin lipids leads to positive curvature, but only at sufficient concentration, below which the lipid prefers negative curvature.

DOI: 10.1103/PhysRevLett.117.138104

Phospholipid surfactants form the major structural component of the membranes that separate aqueous compartments in the cell. A bilayer formed of phospholipids is composed of two oppositely facing *leaflets*, with polar lipid head groups facing the aqueous sides, and an oily interior. The surface is soft and effectively tensionless; it is deformed in cellular processes like endocytosis [1], vesicle fusion [2,3], and viral entry [4]. Specific lipids are thought to substantially stabilize these deformed membranes due to their ability to support nonlamellar phases with porelike character [5–8]. For example, caveolae are pits enriched in lipids such as sphingomyelin, cholesterol, and signaling proteins [9]. How caveolae maintain enriched lipid concentrations, however, remains an open question. A popular hypothesis is that lipid localization is stabilized by the formation of a liquid ordered phase (L_o) [10,11], favored by sphingomyelin and cholesterol. Recent experiments suggest that L_o-like mixtures prefer highly curved membranes [12], offering a mechanism but awaiting a theoretical explanation.

These important biophysical problems—how lipid composition determines the energetics of membrane deformations and how lipids colocalize at specific (curved) locations on the cell surface—are thus of considerable interest for a broad range of physiological processes. Predicting the material properties of the bilayer as its composition is varied is an ideal problem for simulation, as it relies on precisely controlled conditions. Furthermore, one of the main conclusions of this Letter is that the fundamental experiment (the osmotic pressure dependence of the inverse hexagonal lipid phase) used to determine lipid curvature is misleading in important cases [here, cholesterol and palmitoyl sphingomyelin (PSM)]. The underlying reason is fundamental—lipid spontaneous curvatures will frequently not be additive.

The starting point for describing the curvature properties of the bilayer is the Helfrich Hamiltonian [13],

$$\bar{F}_H = \frac{k_c}{2}(c_1 + c_2 - c_0)^2 + k_g c_1 c_2, \tag{1}$$

$$\bar{F}'_H(0) = -k_c c_0, \tag{2}$$

a second-order expansion of the free energy ($\bar{F}_H$) per unit area of a lipid leaflet in terms of the sum and product of the principal curvatures (c_1, c_2) of the surface. The force constant for bending is the bending modulus k_c, k_g is the Gaussian curvature modulus, and c_0 is the spontaneous curvature. Here, k_c and c_0 are defined on a leaflet or monolayer basis, rather than for a whole bilayer. The first derivative of the free energy with respect to total curvature, evaluated at zero curvature, is denoted $\bar{F}'(0)$ and is important because it is an observable of a simulation, and its sign implies that of c_0. The sign convention for c is that positive curvature is convex with respect to the head groups.

The spontaneous curvature displays a wide range depending on lipid type, from highly positively curved for single-tail phospholipids [14] to highly negative for lipids with a phosphatidylethanolamine head group [15]. In applications of the Helfrich Hamiltonian to membrane bending, the additivity assumption for c_0 is ubiquitous; see, e.g., Refs. [16,17]. For a mixture of two lipids, A and B, with fractions f^A and f^B and spontaneous curvatures c_0^A and c_0^B, the spontaneous curvature is

$$c_0^{\text{mix}} = f^A c_0^A + f^B c_0^B. \tag{3}$$

Violation of Eq. (3) indicates clearly that lipid-lipid interactions couple strongly to curvature; i.e., the environment around a lipid affects its curvature preference. A nonadditive effect of cholesterol for saturated or unsaturated chains was previously observed for k_c [18], but the experiment is insensitive to c_0.

This Letter reports two cases of strong nonlinearity in lipid mixtures simulated with the Chemistry at Harvard Macromolecular Mechanics all-atom force field [19], evident as a violation of Eq. (3) confirmed by computing $\bar{F}'(0)$ from Eq. (2). (i) The effect of cholesterol on lipids with saturated chains is dramatically different from that with unsaturated chains. (ii) PSM hydrogen bonding interactions induce positive curvature at high PSM concentrations. Both of these lipids are critical structural components of the plasma membrane.

The distinction between nonlinearity and nonadditivity is subtle. For example, cholesterol may have two *different* linear effects on $\bar{F}'(0)$ at low concentrations, depending on its lipid matrix. Yet, this still could imply that its effect is nonadditive. Observing a nonlinear dependence of $\bar{F}'(0)$ on composition directly contradicts a local, additive model of lipid mixtures. Important distinctions between the locality of lipid properties, linearity, and additivity are discussed in detail in Sec. IV of the Supplemental Material (SM) [20].

Experimentally, the spontaneous curvature c_0 of a lipid is determined by forming the inverse hexagonal phase of the lipid [15]. At zero osmotic stress [32], the curvature observed by x-ray scattering is c_0. Upon addition of small quantities of a test lipid to a host matrix of (typically) dioleoylphosphatidylethanolamine (DOPE), the curvature preference changes [14]. Under the additive assumption, c_0 of the test lipid is obtained. For mixtures violating Eq. (3), the inferred c_0 will depend strongly on the host matrix, yielding values that would be incorrect in a different target membrane composition.

Molecular simulations yield values of $\bar{F}'(0)$ (here, the subscript H is dropped, as the model is no longer restricted to Helfrich) by computing the lateral pressure profile, and then calculating the first moment of a single leaflet via [33,34]

$$\bar{F}'(0) = -\int_0^{L_c/2} z[p_T(z) - p_N(z)]dz(\text{sim}). \qquad (4)$$

The integration is taken from $z = 0$, the bilayer center, to the top of the periodic cell. Note that in terms of the Helfrich Hamiltonian, $\bar{F}'(0)$ is $-k_c c_0$. See Sec. V of the SM for a discussion of how the pressure profile is translated to $\bar{F}'(0)$, Sec. VI for how the profile is calculated, and Sec. VII for an analysis of finite system size effects.

In a simulation, it is simple to change lipid composition, compute $\bar{F}'(0)$, and thus to test Eq. (3). A modest 100 ns simulation (the minimum length used herein) achieves sufficient certainty. This time scale is sufficient for lipids to change their interacting partners multiple times, even in the case of 100% PSM bilayers where the dynamics are slowed.

Before discussing the values of $\bar{F}'(0)$ that indicate the nonadditivity for cholesterol and PSM shown in Figs. 1 and 3, a simple mechanical model of curvature will be presented to interpret the curvature dependence of the lipid-tail ordering effect of cholesterol and of PSM hydrogen bonding.

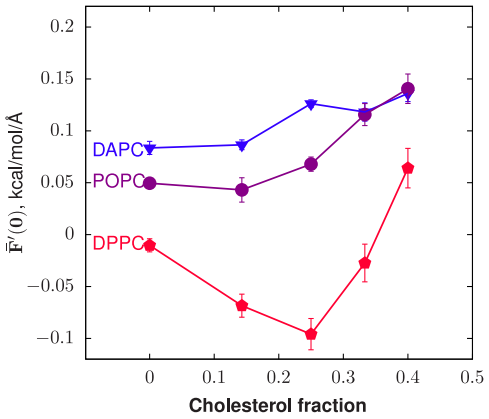

FIG. 1. The derivative of the free energy (per unit area) with respect to curvature versus the cholesterol mole fraction.

Mechanical curvature model.—Consider a minimal description of the stresses in a lipid bilayer with a net cohesive and a net expansive part. The cohesive force is a combination of oily tail attraction and minimization of the hydrophobic-polar surface of the bilayer, with $(dF_{\text{cohesive}}/dA) = \Pi$ being positive; the effect of tail chain entropy acts to expand the surface, with $(dF_{\text{c.e.}}/dA) = -\Pi$ to give zero total surface tension. Below, Π will be estimated using polymer-brush theory, following Ref. [35]. First, it is necessary to estimate how changes in these forces affect $\bar{F}'(0)$.

A pivotal first step is to assign these forces to regions of the bilayer. If the acyl chain contribution is assigned uniformly to the tail region, and the cohesive interaction to a surface dividing the polar and apolar regions (see Sec. I of the SM for details), then, for dioleoylphosphatidylcholine (DOPC), $\bar{F}'(0) = 0.50$ kcal/mol/Å is obtained—about 6 times higher than expected. The discrepancy is likely due to the simplified assignment of the cohesive and expansive interactions. For example, moving part of the cohesive interaction into the tail region under the constraint of zero tension has the effect of reducing the negative curvature propensity of the leaflet; a similar result is obtained by including steric repulsion of head groups.

Rawicz *et al.* experimentally validated a model of the interplay between chain entropy and the cohesive stress Π [36]: polymer-brush theory. Chain confinement is parametrized by x, the ratio of the tail length h_l to its theoretical maximum *all-trans* extension, h_l^0, with $x = (h_l/h_l^0)$ ranging between zero and one. For short chains, Flory showed that the free energy of a confined freely jointed chain is approximately

$$F_{\text{c.e.}} \approx (3k_B T n_s/2)x^2, \qquad (5)$$

accurate up to ≈90% of the maximum chain extension [37]. Assuming incompressibility, the projected area is also related to x by $x = (a_c/a)$, where a value of $a_c = 22.5$ Å^2 is used for the limiting value of the chain area.

Note that none of the conclusions are changed by using a value of 20 Å^2 for a_c, but also that the confinement values x are lowered and values of n_s are increased for each system. The derivative of the chain free energy with respect to area is

$$\frac{dF_{\text{c.e.}}}{da} = -\frac{3k_BTn_s}{a_c}x^3, \tag{6}$$

and within this model is equal to $-\Pi$. The strength of the force is modulated by the degree of confinement (large values of x) and the number of independent units of the polymer (n_s). Note that the quantity n_s is treated as an inherent property of the acyl chain that, when confined, cannot be computed by the standard means of polymer theory [37]. Through interactions with the environment, however, the chain may stiffen, decreasing n_s. For example, cholesterol condenses saturated acyl chains and reduces the number of effectively independent polymer segments and thus reduces lateral stress. The strategy in this Letter is to infer n_s from K_A, as described below.

In Evans's work, Π is determined by a model of the chain free energy, which is balanced by all of the other complex and unknown bilayer stresses that depend linearly on the area. Thus, both the first derivative Π and the second derivative K_A are related to confinement and n_s through

$$K_A = 6\Pi = \frac{n_s 18k_BTx^3}{a_c} \quad \text{(polymer-brush theory)}. \tag{7}$$

The value of n_s can therefore be deduced from K_A by dividing it by $(18k_BTx^3/a_c)$. The value of K_A is, in turn, available from a zero surface tension simulation of a lipid bilayer through the relation [38]

$$K_A = \frac{A_0k_BT}{\langle (A-A_0)^2\rangle}. \tag{8}$$

Note that n_s depends strongly on the limiting value of a_c chosen (directly and through x). Nevertheless, the values of the Kuhn length for the acyl chains of dipalmitoylphosphatidylcholine (DPPC) and for polymethylene melts are roughly equal (approximately 1 nm, or $n_s = 2$). Alternative reasonable choices for a_c do not affect the conclusions of this Letter.

A general conclusion of the polymer-brush model is that, without an enhancement of tail cohesion, increasing Π—and thus increasing K_A—should promote a more positive value of $\bar{F}'(0)$ (implying a stronger negative curvature preference). As shown below, cholesterol in combination with saturated acyl chains violates this trend, which is seen in the other lipids.

Nonadditivity of cholesterol spontaneous curvature.—Figure 1 plots $\bar{F}'(0)$ for mixtures of cholesterol in bilayers of diarachidonyl-PC (DAPC), 1-palmitoyl-2-oleoyl-PC (POPC), and DPPC. Note that, if $\bar{F}'(0)$ is interpreted through the Helfrich Hamiltonian to be $-k_cc_0$, and with k_c necessarily positive, the sign of $\bar{F}'(0)$ is the opposite of that of c_0. For DAPC and POPC, cholesterol induces a stronger negative curvature preference, consistent with inverse hexagonal phase measurements in DOPE and DOPC [39] and implying that cholesterol induces negative curvature. However, in DPPC, cholesterol has a net positive effect on spontaneous curvature for up to 33% cholesterol by mole, implying that cholesterol has *positive* curvature. Because of the different behavior of cholesterol, depending on the presence of saturated acyl chains, it cannot be described by an additive model. Simulations of a liquid ordered phase with a majority DPPC and cholesterol indicate substantial condensation of the acyl chains of DPPC [40], consistent with a reduction of n_s and a strong cohesive force in the tail region.

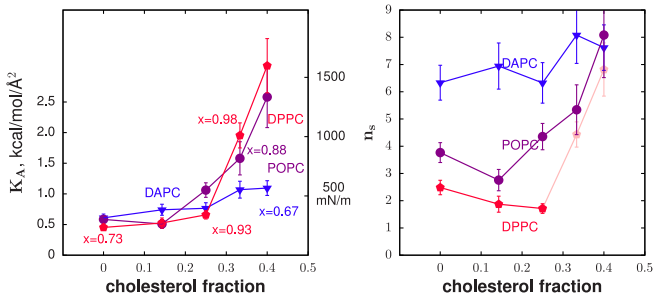

FIG. 2. (Left panel) The area compressibility modulus versus the cholesterol mole fraction from simulation. Selected points are labeled with their chain extension values x, as defined in the text. (Right panel) The number of independent effective polymer segments, n_s, versus the cholesterol mole fraction. Values for DPPC past 0.25 mole fraction cholesterol are dimmed because the Gaussian approximation for the free energy is likely no longer valid in these highly constrained environments.

Figure 2 shows the area compressibility K_A and n_s computed from simulations of phospholipid-cholesterol mixtures. Selected points in the plot of K_A have been labeled with their corresponding value of x, illustrating how the values of K_A for DPPC are low considering how confined the tails are (x is closer to 1). For DPPC, in the regime of applicable x, the number of independent units drops with increasing cholesterol concentration, in contrast to the other lipids simulated.

The polymer-brush model provides a consistent explanation for why cholesterol-rich liquid ordered phases prefer positive curvature relative to disordered phases. Condensing the alkane tails manifests as a reduction in the number of independent polymer segments, as shown by the trend in K_A with confinement. This condensation is driven by the cohesive effect of all-trans alkane chain packing and thus induces positive curvature by creating a cohesive interaction below the neutral surface of bending. As plotted in Sec. III of the SM [20], the lateral pressure profile is consistent with this mechanism.

Cholesterol also drives a positive spontaneous curvature in more complex mixtures of lipids. An L_o mixture of 0.55/0.47/0.30 DPPC/DOPC/Cholesterol [40] obtains a value of $\bar{F}'(0) = -0.116$ kcal/mol/Å, while a mixture of

0.29/0.60/0.11 of the same lipids has more disordered chains—typical of a conventional fluid phase—and $\bar{F}'(0) = 0.05\,\mathrm{kcal/mol/Å}$ (standard error < 0.013 kcal/mol/Å).

Thus, a local variation in membrane composition, as is hypothesized to underlie membrane lateral organization [41], also can change the *sign* of the local spontaneous curvature.

Nonlinearity of sphingomyelin curvature stress.—Figure 3 plots $\bar{F}'(0)$ for mixtures of DOPE and either PSM or DOPC. The red curve shows a quadratic fit $(b + mf + kf^2)$ to the PSM and DOPE values.

The quadratic variation of $\bar{F}'(0)$ by the fraction PSM is -0.42 ± 0.04. As expected, the variation in $\bar{F}'(0)$ for the DOPE/DOPC mixtures is fit well with either linear $(p = 0.34)$ or quadratic $(p = 0.39$, coefficient $k = -0.05)$ models; experiments in the inverse hexagonal phase at relatively high DOPC concentration show no signs of nonadditivity [39]. The high quality of the quadratic fit and small value of the slope m indicates that the curvature preference of PSM is nearly indistinguishable from DOPE at low concentration, consistent with a recent x-ray experiment on PSM in DOPE [43]. The nonlinear variation of $\bar{F}'(0)$ indicates that PSM and DOPE lipid curvature free energetics cannot be interpreted by a local additive model (see Sec. IV of the SM [20]).

Much like the effect of cholesterol on saturated lipids, the molecular explanation is that a cohesive interaction is balanced by an expansive interaction between negatively charged phosphate groups. In this case, however, the cohesive interaction is due to amide-amide hydrogen bonding between PSM backbones. The difference between the lateral pressure profiles of DOPE and PSM shows this quite clearly, with a large cohesive peak near the amide-amide hydrogen bond depth, balanced by a repulsion above (see Fig. S1 of the SM [20]). The explanation for the balance between amide cohesion and phosphate repulsion is further justified by replacing a portion of the phosphatidylcholine head groups with hydroxyls to form ceramide. In simulations conducted at 340 K, $\bar{F}'(0)$ for PSM-ceramide mixtures of 0%, 5%, 10%, and 20% ceramide is -0.088, -0.057, -0.012, and 0.105 kcal/mol/Å, respectively (s.e. < 0.011 kcal/mol/Å). That is, the positive curvature effect of sphingomyelin is rapidly removed and replaced with strong negative curvature. The lack of a strong repulsion to balance the cohesive effect of the amide hydrogen bond (and thus to maintain fluidity) is clear from the phase behavior of ceramide, which induces gel phase domains even at low fractions [44].

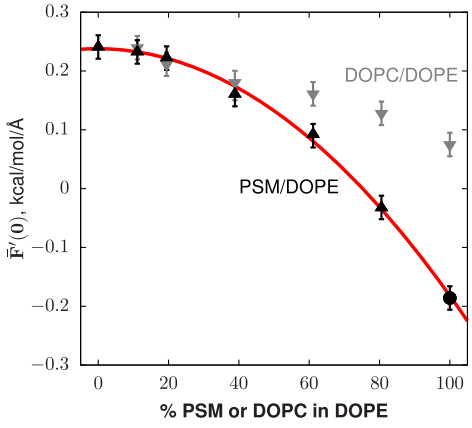

FIG. 3. The derivative of the free energy (per unit area) with respect to curvature. The 100% PSM point indicated by the circle (taken from a previous study [42]) was run at 321 K, while the others were run at 318 K.

An alternative explanation for the data in Fig. 3 is that the spontaneous curvature is additive, but that it is the globally averaged values of k_c and c_0 that determine $\bar{F}'(0)$. While this model cannot be ruled out without an independent, rigorous calculation of the bending modulus for the mixture, it requires small concentrations of PSM to influence the k_c of DOPE nonlocally and thus increase the negative curvature strain of DOPE. This is discussed at length in Sec. IV of the SM [20].

The nonlinear behavior of c_0 for the PSM mixture resolves two experiments that appear to be in disagreement. Nuclear magnetic resonance experiments on small lipid vesicles indicate that sphingomyelin prefers the positively curved outer leaflet [45,46], consistent with a positive value of c_0. In contrast, x-ray crystallography of mixtures of sphingomyelin and DOPE in the inverse hexagonal phase at a low sphingomyelin concentration (10% or less) show that sphingomyelin has a weak effect on the negative c_0^{mix} of the mixture [43], indicating that it also has a negative curvature preference (though somewhat weaker than a PE lipid). The simulations and the theoretical analysis in this Letter resolve this discrepancy, predicting that PSM behaves much like a standard glycero-PC lipid at low concentration, yet it develops a positive c_0 when concentrations of PSM-PSM complexes become specific. The effect may be enhanced by tail condensation of PSM, much like the case with cholesterol.

The value of $\bar{F}'(0)$ cannot distinguish between two possible models of curvature energetics of a mixture:

$$F_{H,l} = \sum_i f_i \int \frac{k_c}{2}(c - c_{0,i})^2 \quad \text{(local)}, \tag{9}$$

$$F_{H,g} = \int \frac{k_c}{2}\left(c - \sum_i f_i c_{0,i}\right)^2 \quad \text{(global)}, \tag{10}$$

as they have the same derivative with respect to c but differ in the chemical potential of lipid i in the leaflet. Here, f_i is the fraction of lipid i in the leaflet, and $c_{0,i}$ is the spontaneous curvature of lipid i. The local model is called this, as the energetics are invariant even if f_i is computed individually for small patches. The difference is critical for interpreting the influence of curvature stress on, for example, the relative lipid composition of the inner and outer leaflets of the plasma membrane (see Ref. [17], in which $F_{H,g}$ was used). Although not apparent from $\bar{F}'(0)$, it follows from our proposed local molecular mechanisms that it is the *local* lipid composition that determines energetics, rather than the global concentration. Thus,

$F_{H,l}$ is appropriate for describing the curvature dependence of the interactions between, e.g., sphingomyelin, with $c_{0,i}$ determined by local composition.

In summary, a theoretical analysis of simulations of lipid mixtures demonstrates that lipid spontaneous curvatures are frequently nonadditive. Changes in lipid composition can have dramatic effects, including changing the sign of the spontaneous curvature. The assumption of additivity underlies a widely used analysis of experimental data to determine spontaneous curvature, so the present results need to be taken into account when analyzing such data. The results also have implications for cellular function, by providing a mechanism to couple complex membrane composition to the partitioning [47] and conformation [48] of integral membrane proteins.

The SM contains a list of simulations, simulation methodology, and other topics already noted in the text [20].

This research was supported by the Intramural Research Program of the National Institutes of Health (NIH), the National Heart, Lung, and Blood Institute (NHLBI), and the Eunice Kennedy Schriver National Institute of Child Health and Human Development. It used the NHLBI LoBoS cluster. E. L. was partially supported by NIH Grant No. P20GM104316-01. Anton computer time to construct the L_o and L_d ensembles was provided by the National Resource for Biomedical Supercomputing (NRBSC), the Pittsburgh Supercomputing Center (PSC), and the BTRC for Multiscale Modeling of Biological Systems (MMBioS) through Grant No. P41GM103712-S1 from the NIH. Feedback from anonymous reviewers of the work substantially enriched the interpretation of the data.

*Corresponding author.
alexander.sodt@nih.gov
Present address: Eunice Kennedy Schriver National Institute of Child Health and Human Development, National Institutes of Health, Bethesda, MD, USA.

[1] G. J. Doherty and H. McMahon, Annu. Rev. Biochem. **78**, 857 (2009).
[2] R. B. Sutton, D. Fasshauer, R. Jahn, and A. T. Brunger, Nature (London) **395**, 347 (1998).
[3] A. Grafmüller, J. Shillcock, and R. Lipowsky, Phys. Rev. Lett. **98**, 218101 (2007).
[4] S. C. Harrison, Nat. Struct. Mol. Biol. **15**, 690 (2008).
[5] D. P. Siegel, W. J. Green, and Y. Talmon, Biophys. J. **66**, 402 (1994).
[6] D. P. Siegel and M. M. Kozlov, Biophys. J. **87**, 366 (2004).
[7] Y. Kozlovsky, A. Efrat, D. Siegel, and M. M. Kozlov, Biophys. J. **87**, 2508 (2004).
[8] S. Aeffner, T. Reusch, B. Weinhausen, and T. Salditt, Proc. Natl. Acad. Sci. U.S.A. **109**, E1609 (2012).
[9] S. Sonnino and A. Prinetti, FEBS Lett. **583**, 597 (2009).
[10] E. J. Shimshick and H. M. McConnell, Biochemistry **12**, 2351 (1973).
[11] J. H. Ipsen, G. Karlström, O. G. Mouritsen, H. Wennerström, and M. J. Zuckermann, Biochim. Biophys. Acta **905**, 162 (1987).
[12] J. B. Larsen, M. B. Jensen, V. K. Bhatia, S. L. Pedersen, T. Bjørnholm, L. Iversen, M. Uline, I. Szleifer, K. J. Jensen, N. S. Hatzakis, and D. Stamou, Nat. Chem. Biol. **11**, 192 (2015).
[13] W. Helfrich, Z. Naturforsch. **28**, 693 (1973).
[14] N. Fuller and R. P. Rand, Biophys. J. **81**, 243 (2001).
[15] R. P. Rand, N. L. Fuller, S. M. Gruner, and V. A. Parsegian, Biochemistry **29**, 76 (1990).
[16] M. Frewein, B. Kollmitzer, P. Heftberger, and G. Pabst, Soft Matter **12**, 3189 (2016).
[17] H. Giang and M. Schick, Biophys. J. **107**, 2337 (2014).
[18] J. Pan, T. T. Mills, S. Tristram-Nagle, and J. F. Nagle, Phys. Rev. Lett. **100**, 198103 (2008).
[19] J. B. Klauda, R. M. Venable, J. A. Freites, J. W. O'Connor, D. J. Tobias, C. Mondragon-Ramirez, I. Vorobyov, A. D. Mackerell, Jr., and R. W. Pastor, J. Phys. Chem. B **114**, 7830 (2010).
[20] See Supplemental Material at http://link.aps.org/supplemental/10.1103/PhysRevLett.117.138104, which includes Refs. [21–31], for an expanded discussion of the computation of $\bar{F}'(0)$ and its interpretation.
[21] A. J. Sodt and R. W. Pastor, Biophys. J. **104**, 2202 (2013).
[22] T. Baumgart, S. T. Hess, and W. W. Webb, Nature (London) **425**, 821 (2003).
[23] R. M. Venable, F. L. H. Brown, and R. W. Pastor, Chem. Phys. Lipids **192**, 60 (2015).
[24] P. Schofield and J. R. Henderson, Proc. R. Soc. A **379**, 231 (1982).
[25] L. D. Landau and E. M. Lifshitz, *Theory of Elasticity* (Pergamon, New York, 1970).
[26] E. Lindahl and O. Edholm, J. Chem. Phys. **113**, 3882 (2000).
[27] J. Sonne, F. Y. Hansen, and G. Peters, J. Chem. Phys. **122**, 124903 (2005).
[28] B. S. Perrin, A. J. Sodt, M. L. Cotten, and R. W. Pastor, J. Membr. Biol. **248**, 455 (2015).
[29] T. Darden, D. York, and L. Pedersen, J. Chem. Phys. **98**, 10089 (1993).
[30] H. C. Andersen, J. Comput. Phys. **52**, 24 (1983).
[31] S. E. Feller, Y. Zhang, R. W. Pastor, and B. R. Brooks, J. Chem. Phys. **103**, 4613 (1995).
[32] S. M. Gruner, V. A. Parsegian, and R. P. Rand, Faraday Discuss. Chem. Soc. **81**, 29 (1986).
[33] I. Szleifer, D. Kramer, A. Ben-Shaul, W. Gelbar, and S. A. Safran, J. Chem. Phys. **92**, 6800 (1990).
[34] R. Goetz and R. Lipowsky, J. Chem. Phys. **108**, 7397 (1998).
[35] J. Pan, S. Tristram-Nagle, N. Kućerka, and J. F. Nagle, Biophys. J. **94**, 117 (2008).
[36] W. Rawicz, K. C. Olbrich, T. McIntosh, D. Needham, and E. Evans, Biophys. J. **79**, 328 (2000).
[37] P. J. Flory, *Statistical Mechanics of Chain Molecules* (Interscience, New York, 1969).
[38] L. D. Landau and E. M. Lifshitz, *Statistical Physics*, Vol. 5 (Pergamon, New York, 1970), Sec. 114.
[39] Z. Chen and R. P. Rand, Biophys. J. **73**, 267 (1997).
[40] A. J. Sodt, M. L. Sandar, K. Gawrisch, R. W. Pastor, and E. Lyman, J. Am. Chem. Soc. **136**, 725 (2014).

[41] K. Simons and E. Ikonen, Nature (London) **387**, 569 (1997).
[42] R. M. Venable, A. J. Sodt, B. Rogaski, H. Rui, E. Hatcher, A. D. Mackerell, R. W. Pastor, and J. B. Klauda, Biophys. J. **107**, 134 (2014).
[43] B. Kollmitzer, P. Heftberger, M. Rappolt, and G. Pabst, Soft Matter **9**, 10877 (2013).
[44] L. Silva, R. de Almeida, A. Fedorov, A. Matos, and M. Prieto, Molecular membrane biology **23**, 137 (2006).
[45] J. A. Berden, R. W. Barker, and G. K. Radda, Biochim. Biophys. Acta **375**, 186 (1975).
[46] P. Mattjus, B. Malewicz, J. T. Valiyaveettil, W. J. Baumann, R. Bittman, and R. E. Brown, J. Biol. Chem. **277**, 19476 (2002).
[47] J. H. Lorent and I. Levental, Chem. Phys. Lipids **192**, 23 (2015).
[48] O. Soubias, W. E. Teague, K. G. Hines, D. C. Mitchell, and K. Gawrisch, Biophys. J. **99**, 817 (2010).